INTERNATIONAL JOURNAL FOR NUMERICAL METHODS IN FLUIDS, VOL. 21, 15–34 (1995)

# A SIMPLIFIED MARKER AND CELL METHOD FOR UNSTEADY FLOWS ON NON-STAGGERED GRIDS

LIANG CHENG

*Department of Civil Engineering, The University of Western Australia, Nedlands, W.A. 6009, Australia*

AND

STEVEN ARMFIELD

*Centre for Advanced Numerical Computation in Engineering and Science, University of New South Wales, Sydney, N.S.W. 2052, Australia*

SUMMARY

The SMAC (simplified marker and cell) time-advancing method for solving the unsteady incompressible Navier–Stokes equations on non-staggered grids is developed in generalized co-ordinate systems. The primitive variable formulation uses Cartesian velocities and pressure, all defined at the centre of the control volume, as the dependent variables. A special elliptic flux correction at the faces of the finite volume is utilized in discretizing the continuity equation to suppress pressure oscillations. The test flows considered are a polar cavity flow starting from rest and the flow around a circular cylinder. The numerical results are compared with experimental results and results obtained by the well-known SIMPLEC and PISO methods. The comparisons show that the elliptic flux correction technique works well in suppressing pressure oscillations and that the SMAC method is more efficient than the SIMPLEC and PISO methods for both steady and unsteady flows.

KEY WORDS: SMAC; curvilinear co-ordinates; non-staggered grids; elliptic correction

## 1. INTRODUCTION

With the rapid increase in computer power available to the researcher, there is an increasing need for solving incompressible unsteady flows in complex domains. This need has motivated the intensive development of numerical methods for solving the Navier–Stokes equations in curvilinear co-ordinate systems. Several alternative curvilinear grid approaches have been reported in the literature.[1–3] Most of these methods use staggered grid arrangements whereby the dependent variables are not stored at the same locations. A minority use non-staggered grids in which all the dependent variables are stored at the same location. The purpose of the present research is to extend the existing methods and develop and validate an unsteady viscous incompressible flow solver using primitive variables on a non-staggered curvilinear co-ordinate system. The ultimate result of the present work is to develop a solution technique that can be used to compute complex 3D incompressible flows; however, this paper will be limited to the 2D case.

As noted above, most schemes reported in the literature use staggered grid arrangements. The reason is that the use of a non-staggered grid can result in an undesirable grid-scale oscillation in the pressure field. Staggered grids, in which the velocities are stored at locations offset from the pressure, prevent

CCC 0271–2091/95/010015–20

*Received 27 September 1993*
*Revised 14 September 1994*

this checkerboard effect by using any change in the pressure field at adjacent grid locations to drive the velocity. Despite this disadvantage of non-staggered grids, they do have many advantages when compared with the staggered grid, as follows.[2]

(i) All variables share the same location; hence there is only one set of control volumes.
(ii) The convection contribution to the coefficients in the discretized equations is the same for all variables.
(iii) For complex geometries, Cartesian velocity components can be used in conjunction with non-orthogonal co-ordinates, yielding simpler equations than when co-ordinate-oriented velocity components are employed.
(iv) There are fewer constraints on the numerical grid, since there is no need to evaluate the so-called 'curvature terms'.

Provided that the pressure checkerboard problem can be eliminated, the non-staggered arrangement has much to recommend it. One method of eliminating the pressure oscillations is to use higher-order dependent variables such as streamfunction and vorticity. However, the order of the equations is then increased, with adverse effects on computational efficiency, and the specification of the vorticity boundary conditions is not straightforward. Owing to the difficulties associated with using higher-order dependent variables and the advantages of using non-staggered grids if the pressure oscillation can be eliminated, in the present project a primitive variable scheme defined on a non-staggered mesh with non-orthogonal curvilinear co-ordinates is being developed.

Over the past 10 years, several non-staggered schemes for primitive variables have been developed. Rhie and Chow[4] have presented a steady solution method which employs a non-staggered grid in the framework of non-orthogonal curvilinear co-ordinates. The scheme utilizes the SIMPLE approach of Patankar and Spalding.[5] The key idea in Rhie and Chow's method is to use an interpolation for calculating the flux through the faces of the control volume using the discretized momentum equations for two adjacent control volumes separated by the face in question. The method has been applied to a number of steady flows[6,7] and effectively eliminates the pressure oscillation. In the method developed by Reggio and Camarero,[8] which is also based on SIMPLE, staggering is introduced in the differencing formulae rather than in the grid. Forward differencing is used for the mass flow rate and backward differencing for the pressure gradients.

Both the Rhie–Chow[4] and Reggio–Camarero[8] methods can be used to solve unsteady incompressible flows. However, since both methods are based on the SIMPLE algorithm which was initially developed for steady incompressible flows, they may not be ideally suited to unsteady calculations. A number of researchers have considered alternative non-iterative strategies for the solution of unsteady problems.

One of the earliest and most widely used methods for solving time-dependent incompressible flows is the MAC (marker and cell) method of Harlow and Welch.[9] The method solves a Poisson equation for the pressure and the momentum equations for the velocities once at each time step and is defined on a staggered grid. The method was initially proposed for unsteady flows involving free surfaces and then used as a method for solving incompressible unsteady flows.

An alternative formulation called the simplified marker and cell method (SMAC) was later proposed by Amsden and Harlow.[10] In the SMAC method at each time step tentative velocities are first obtained by solving the momentum equations. These initial velocities, which may not satisfy mass conservation, are modified in such a way as to preserve the vorticity but bring the divergence to zero. This is accomplished by setting the difference between final and initial velocities equal to the gradient of a potential function. The potential function is then found by solving a Poisson equation for which the boundary conditions are strictly homogeneous. Thus SMAC requires fewer boundary conditions and eliminates the boundary inhomogeneities of the original Poisson pressure equation, allowing for a

more efficient solution. More recently the SMAC method has been utilized by Kim and Benson[1] for solving the unsteady incompressible Navier–Stokes equation in non-orthogonal curvilinear co-ordinates using a staggered grid with primitive variables. The SMAC method is compared numerically with the SIMPLE and PISO[11] methods for a few test problems in Kim and Benson's work. It is concluded according to their numerical results that for a larger time step SMAC and SIMPLE are more strongly convergent and yield more accurate results than the PISO scheme and that SMAC is the most efficient computationally.

For comparison purposes the well-known SIMPLEC[12] and PISO[11] methods have also been coded on non-staggered grids in the present model. The numerical results of a few test problems obtained by these methods will be compared with each other and with experimental results, allowing the accuracy and efficiency of the SMAC method to be evaluated. To prevent the grid-scale pressure oscillation described above from occurring, an elliptic flux correction method described by Armfield[13] is used in all three methods. Armfield proposed a scheme of the same type as the Rhie–Chow scheme for an unsteady problem with a rectangular co-ordinate system but without the relaxation error identified by Majumdar.[6] Armfield further demonstrated that schemes of this type effectively introduce an additional discrete term into the continuity equation which leads to the non-staggered scheme having an identical discrete ellipticity to the standard staggered SIMPLE scheme. Without the additional term, non-staggered schemes are non-elliptic at the grid-scale wave number, resulting in the pressure oscillations described above. In a later paper Armfield[14] showed that the additional term introduces an additional second-order truncation error but that at least for the flow considered the additional error did not significantly degrade the accuracy of the scheme.

The remainder of the paper is as follows. In Section 2 the governing equations in curvilinear form are presented. The discretization procedure including elliptic flux correction terms and the SMAC method are given in Section 3. The results obtained from the SMAC, SIMPLEC and PISO methods are compared with each other and with experimental results in Section 4. Conclusions are given in Section 5.

## 2. GOVERNING EQUATIONS

The equations governing laminar, incompressible fluid flow are written in conservation Cartesian tensor form as

$$\frac{\partial u_j}{\partial x_j} = 0, \tag{1}$$

$$\frac{\partial u_i}{\partial t} + \frac{\partial}{\partial x_j}\left(u_i u_j - \frac{1}{Re}\frac{\partial u_i}{\partial x_j}\right) = -\frac{\partial p}{\partial x_i}, \tag{2}$$

where $u_j$ is the Cartesian velocity component, $p$ is the pressure and $Re$ is the Reynolds number. The summation rule for repeated indices is implied in the above equations.

For the numerical analysis it is more convenient to write the above equations in a general dimensionless form as

$$\frac{\partial \phi}{\partial t} + \frac{\partial}{\partial x_j}\left(u_j \phi - \Gamma \frac{\partial \phi}{\partial x_j}\right) = S^{\phi}, \tag{3}$$

where $\phi$ stands for the dimensionless variables (i.e. when $\phi = u_i$, equation (3) corresponds to equation (1) or (2) respectively) and $\Gamma$ and $S^{\phi}$ are the dimensionless forms of the diffusion coefficient and the source term respectively.

The conservative form of equation (3) in the non-orthogonal curvilinear co-ordinate system $(\xi, \eta)$ can be obtained by introducing the transformation relations

$$\xi = \xi(x,y), \qquad \eta = \eta(x,y), \tag{4}$$

$$f_x = (y_\eta f_\xi - y_\xi f_\eta)/J, \qquad f_y = (-x_\eta f_\xi + x_\xi f_\eta)J \tag{5}$$

into equation (3) to give

$$\begin{aligned}\frac{\partial \phi}{\partial t} + \frac{1}{J}\frac{\partial}{\partial \xi}(U\phi) + \frac{1}{J}\frac{\partial}{\partial \eta}(V\phi) = &\frac{1}{J}\frac{\partial}{\partial \xi}\left[\frac{\Gamma}{J}\left(\alpha\frac{\partial \phi}{\partial \xi} - \beta\frac{\partial \phi}{\partial \eta}\right)\right] \\ &+ \frac{1}{J}\frac{\partial}{\partial \eta}\left[\frac{\Gamma}{J}\left(\gamma\frac{\partial \phi}{\partial \eta} - \beta\frac{\partial \phi}{\partial \xi}\right)\right] + S^\phi(\xi, \eta),\end{aligned} \tag{6}$$

where

$$J = x_\xi y_\eta - x_\eta y_\xi, \tag{7}$$

$$U = uy_\eta - vx_\eta, \qquad V = vx_\xi - uy_\xi, \tag{8}$$

$$\alpha = x_\eta^2 + y_\eta^2, \qquad \beta = x_\xi x_\eta + y_\xi y_\eta, \qquad \gamma = x_\xi^2 + y_\xi^2, \tag{9}$$

with $u$ and $v$ are Cartesian velocity components in $x$ and $y$ respectively.

Integrating equation (6) over a finite volume element, the following integral conservation relation is then obtained:

$$\begin{aligned}\int\int_R \frac{\partial \phi}{\partial t} J \, \mathrm{d}\xi \, \mathrm{d}\eta + \int_B (U\phi \, \mathrm{d}\eta - V\phi \, \mathrm{d}\xi) \\ = \int_B \left(\frac{\Gamma}{J}(\alpha\phi_\xi - \beta\phi_\eta)\, \mathrm{d}\eta - \frac{\Gamma}{J}(\gamma\phi_\eta - \beta\phi_\xi)\, \mathrm{d}\xi\right) \\ + \int\int_R JS^\phi \mathrm{d}\xi \, \mathrm{d}\eta,\end{aligned} \tag{10}$$

where the integration subscripts $R$ and $B$ indicate the area $R$ and the boundary of $R$ respectively.

## 3. NUMERICAL METHODS

### 3.1. *Grid arrangement and discretization*

The non-orthogonal curvilinear grid on which the 2D unsteady incompressible Navier–Stokes equations are solved can be generated either by using the body-fitted co-ordinate technique proposed by Thompson *et al.*[15] or by algebraic methods. The type of control volume and the variable arrangement used in the present method are shown in Figure 1. All variables and flow properties are defined at the geometric centre (P) of the control volume. The four neighbouring control volume centres are indicated by N, S, E and W for the north, south, east and west neighbours. The interface centres of the control volumes are marked by n, s, e and w respectively. The discretized form of equation (10) can be obtained by integrating it over control volume P:

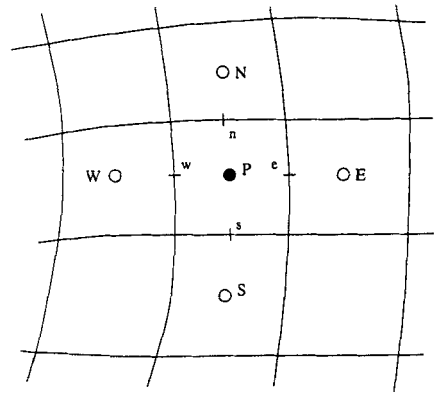


Figure 1. Layout of a control volume

$$\frac{\partial \phi}{\partial t}\Delta\xi\,\Delta\eta + (U\phi\Delta\eta)_{\mathrm{w}}^{\mathrm{e}} + (V\phi\Delta\xi)_{\mathrm{s}}^{\mathrm{n}} = \left(\frac{\Gamma}{J}(\alpha\phi_\xi - \beta\phi_\eta)\Delta\eta\right)_{\mathrm{w}}^{\mathrm{e}} + \left(\frac{\Gamma}{J}(\gamma\phi_\eta - \beta\phi_\xi)\Delta\xi\right)_{\mathrm{s}}^{\mathrm{n}} + JS^\phi\Delta\xi\,\Delta\eta. \tag{11}$$

In the present study the temporal variation of equation (11) is approximated by a first-order backward difference and the diffusion and convection terms are discretized by central differences and the QUICK[16] scheme respectively. Incorporating these approximations into equation (11), a relation between $\phi_{\mathrm{P}}$ and the neighbouring values is obtained:

$$(1 + A_{\mathrm{P}})\phi_{\mathrm{P}} = \sum_{nb} A_k\phi_k + S_{\mathrm{P}}. \tag{12}$$

In the above equation $S_{\mathrm{P}}$ is the new source term which includes the extra terms dropped from the transient term and diffusion terms in the process of discretization of equation (12); *nb* stands for the neighbouring points of P.

### *3.2. Simplified marker and cell method*

In the SMAC method a tentative velocity field is obtained by solving the momentum equations based on the flow variables at the previous time level:

$$(1 + A_{\mathrm{P}}^{n-1})u_{\mathrm{P}}^* = \sum_{nb} A_k^{n-1}u_k^* + S_{\mathrm{P}}^u + (B^u p_\xi^{n-1} + C^u p_\eta^{n-1}), \tag{13}$$

$$(1 + A_{\mathrm{P}}^{n-1})v_{\mathrm{P}}^* = \sum_{nb} A_k^{n-1}v_k^* + S_{\mathrm{P}}^v + (B^v p_\xi^{n-1} + C^v p_\eta^{n-1}), \tag{14}$$

where $B^u, C^u, B^v$ and $C^v$ are the discrete pressure coefficients and $S_{\mathrm{P}}^u$ and $S_{\mathrm{P}}^v$ are the source terms from which the pressure gradient terms have been extracted. The superscript asterisk on $u$ and $v$ denotes that they are the tentative velocities. The tentative velocities obtained using equations (13) and (14) may not satisfy the continuity constraint and must be modified. The tentative velocity field $(u^*, v^*)$ is transformed to the final velocity $(u^{n+1}, v^{n+1})$ using a vorticity preserving auxiliary potential

function $\psi$ such that

$$u_i^{n+1} = u_i^* - \frac{\partial \psi}{\partial x_i}. \tag{15}$$

By substituting equation (15) into equation (11) and letting $\psi = 1$ in equation (11), a discretized equation for $\psi$ is obtained:

$$(U^* \Delta \eta)_w^e + (V^* \Delta \xi)_s^n = \left(\frac{1}{J}(\alpha \psi_\xi - \beta \psi_\eta)\Delta \eta\right)_w^e + \left(\frac{1}{J}(\gamma \psi_\eta - \beta \psi_\xi)\Delta \xi\right)_s^n. \tag{16}$$

After $\psi$ has been calculated from equation (16), the divergence-free velocity field at time $n+1$ is evaluated according to equation (15). The corresponding pressure is obtained by subtracting the momentum equation at the tentative level from the momentum equation at time $n+1$:

$$\frac{\partial p^{n+1}}{\partial x_i} = \frac{\partial}{\partial x_i}\left(p^n + \frac{\psi}{\Delta t}\right) - \frac{\partial}{\partial x_j}\left(u_j^n \frac{\partial \psi}{\partial x_i}\right) + \frac{1}{Re}\frac{\partial \psi}{\partial x_j \partial x_j}\left(\frac{\partial \psi}{\partial x_i}\right). \tag{17}$$

To solve equation (17), it is assumed that the second term (convection term) on the right-hand side is negligible, allowing an approximate solution $p^{n+1}$ to be obtained as

$$p^{n+1} = p^n + \frac{\psi}{\Delta t} - \frac{1}{Re}\frac{\partial^2 \psi}{\partial x_j \partial x_j}. \tag{18}$$

This approximation has been reported to be reasonable for $Re \leq 1000$ by Braza *et al.*[17] and Kim and Benson.[2]

Relations (15), (16) and (18) are only used at interior mesh points. At boundary points the velocity boundary conditions are specified directly and the pressure boundary conditions are then obtained from the momentum equations on the boundary.

It is well known if $(U^*)_w^e$ and $(V^*)_s^n$ in equation (16) are approximated simply by linear interpolation of the neighbouring node values on the non-staggered grid, an oscillatory pressure field will result. This has been discussed in Rhie and Chow's work.[4] To solve this problem, Rhie and Chow[4] used a special interpolation technique called momentum interpolation.[6] This method works well for steady state problems after modification.[6,7] For some test cases the method[4] has been observed to show better convergence behaviour than the original SIMPLE method. In Armfield's work[13] the problem is solved by using a corrected linear interpolation. The correction terms are composed of a combination of a compact pressure difference and a sparse pressure difference. A theoretical analysis in Reference 13 shows that these correction terms result in a strongly elliptic scheme and that good convergence may be expected, as has been observed for unsteady natural convection in a square cavity. For simplification, only the case of $U_e^*$ is discussed below.

As defined in equation (8), $U_e^*$ can be written as

$$U_e^* = u_e^*(y_\eta)_e - v_e^*(x_\eta)_e. \tag{19}$$

The velocities $u_e^*$ and $v_e^*$ have been used as the advective velocities in equation (11), although it was found that this did not produce any significant variation in the solution. The velocities $u_e^*$ and $v_e^*$ can be expressed as

$$u_e^* = \bar{u}_e + r_e^u, \qquad v_e^* = \bar{v}_e + r_e^v, \tag{20}$$

with the $r$-terms defined as

$$r_e^u = \left[-\overline{(B^u p_\xi^{n-1} + C^u p_\eta^{n-1})} + (\overline{B^u} p_\xi^{n-1} + \overline{C^u} p_\eta^{n-1})_e\right] \Big/ \left(1 + \overline{A}^{n-1}\right),$$

$$r_e^v = \left[-\overline{(B^v p_\xi^{n-1} + C^v p_\eta^{n-1})} + (\overline{B^v} p_\xi^{n-1} + \overline{C^v} p_\eta^{n-1})_e\right] \Big/ \left(1 + \overline{A}^{n-1}\right),$$

where the overbar denotes the linear interpolation between nodes P and E.

The correction terms defined result in the flux through the faces of the control volume being driven by a $1\Delta\xi$ pressure difference rather than a $2\Delta\xi$ pressure difference. This effectively eliminates the pressure oscillations which in the traditional non-staggered methods originate from the $2\Delta\xi$ pressure gradient discretization.

The standard SIMPLEC[18] and PISO[11] methods have also been coded on the non-staggered grid using the elliptic correction described above. The methods will not be described in detail here.

### *3.3. Boundary and initial conditions.*

The boundary conditions that need to be specified in the present problem include velocity boundary conditions, auxiliary potential boundary conditions and pressure boundary conditions. The boundary types considered are the inflow boundary, no-slip wall boundary and open (or outflow) boundary. On the solid wall and inlet boundaries the velocities are known, a zero normal gradient of $\psi$ is prescribed and the pressure is obtained by applying the momentum equation in the direction normal to the boundary. All the first-order derivatives along boundaries are evaluated using second-order, one-sided difference approximations, while the second-order derivatives along boundaries are approximated using first-order, one-sided differences to maintain the numerical consistency.[19] In this way no fictitious points outside the computation domain are needed in the specification of the boundary conditions. For the open boundary the specification of the boundary conditions is not as straightforward as for the inflow and no-slip wall boundaries. The condition $\partial\phi/\partial n = 0$ is often used for open boundaries, where $\phi$ stands for any dependent variable. Unfortunately, this condition does not work well for the present model, as described by Gresho.[19] For the present code a zero value of $\psi$ and the following conditions for velocity and pressure on the open boundary have been found to work well:

$$P = \upsilon \frac{\partial u_n}{\partial n}, \tag{22}$$

$$\frac{\partial \phi}{\partial t} + \bar{u}\frac{\partial \phi}{\partial n} = 0, \tag{23}$$

where $\phi$ is any of the velocity components and $\bar{u}$ is a representative value of the normal velocity at the exit.

An initial divergence-free velocity field is generated by using the method suggested by Gresho,[19] which will not be reported here. The initial pressure field is obtained by solving a Poisson equation which is derived from the initial momentum equations,[19]

$$\frac{\partial^2 p^0}{\partial x_i \partial x_i} = \frac{\partial}{\partial x_i}\left(-u_j^0 \frac{\partial u_i^0}{\partial x_j}\right), \tag{24}$$

with boundary conditions specified as

$$\frac{\partial p^0}{\partial n} = \frac{1}{Re}\left(\frac{\partial^2 u_\tau^0}{\partial \tau^2} + \frac{\partial^2 u_n^0}{\partial n^2}\right) - \frac{\partial}{\partial \tau}(u_n^0 u_\tau^0) - \frac{\partial}{\partial n}(u_n^0 u_n^0) = \frac{\partial u_n^0}{\partial t} \tag{25}$$

on the known velocity boundaries and

$$p^0 - \frac{1}{Re}\frac{\partial u_n^0}{\partial n} \tag{26}$$

on the open boundary where $n$ and $\tau$ are the directions perpendicular and parallel to the boundary. It has been observed that an improperly described initial pressure condition will cause temporal oscillations in the velocity field for the unsteady flow.

## 4. NUMERICAL RESULTS

Numerical results for a polar cavity flow starting from rest and the flow around a circular cylinder at $Re = 40$, 100 and 3000 are presented to validate the procedure proposed in this paper. All the discretized equations were solved by the Gauss–Seidel SOR method.

To facilitate comparisons of the numerical results obtained using different methods, some convergence criteria have been defined. Since the discretized equations are solved iteratively using the SOR method, one set of convergence criteria needs to be prescribed for the SOR iteration:

$$| e |_l^1 = | R_l^k | < \epsilon_l^1, \tag{27}$$

where $l = u, v$ or $\psi$, $R^k$ is the absolute residual of the discrete equation averaged by the number of grid points, evaluated at the $k$th iteration of the SOR, and $\epsilon_l^1$ is the convergence criterion for the $l$th flow variable. For the SIMPLEC method another set of convergence criteria is needed for the iterative solution of the flow equations. The error norm used for the SIMPLEC method is described as

$$|e|^2 = \sum_{i,j} |\mathrm{Div}_{i,j}| / N_{\mathrm{con}} < \varepsilon^2, \tag{28}$$

where $| \mathrm{Div}_{i,j} |$ is the absolute divergence of the $(i,j)$th control volume and $N_{\mathrm{con}}$ is the total number of control volumes. A maximum iteration number is also set to economize the calculations. The convergence criteria used are $| e |^1 = \{1 \times 10^{-7}, 1 \times 10^{-7}, 1 \times 10^{-6}\}$ and $| e |^2 = \{1 \times 10^{-7}\}$. The maximum numbers of SOR iterations for the SMAC and PISO methods are 11, 11 and 100 for the discrete $u$-, $v$- and $p$-equation respectively, while those for SIMPLEC are 5,5 and 11 respectively. The maximum iteration number for the velocity–pressure coupling at each time step in SIMPLEC is 11.

For steady state flows another convergence criterion is needed to determine when a stationary solution is achieved:

$$| e |^3 = \max(| A_{k,l}^n - A_{k-1,l}^n |) / \Delta t < \epsilon^3, \tag{29}$$

where $A_{k,l}^n$ is the $l$th velocity component at the $k$th iteration of the solution of the coupled momentum equations and continuity equation, $\Delta t$ is the time step and $\epsilon^3 = 2 \times 10^{-4}$ is used in the present research.

### *4.1. Polar cavity flow starting from rest*

The lid-driven polar cavity flow has been used as a test problem for numerical algorithms in several studies.[1,3]. The geometrical parameters of the flow are shown schematically in Figure 2, the flow is calculated at $Re = 350$, based on the lid velocity and the depth of the cavity. It is experimentally known that a steady state exists for the polar cavity flow at this Reynolds number.[20] The flow domain is discretized by an $81 \times 81$ grid which is idential with the grid used in Reference 1.

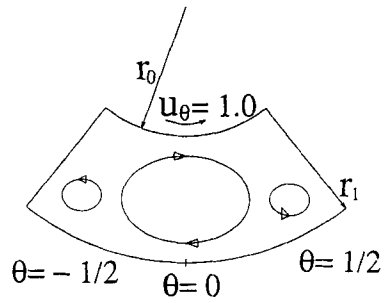


Figure 2. Geometry of polar cavity flow

The flow is simulated using the SMAC, SIMPLEC and PISO methods. The numerical solution of the flow starts with zero velocity field and is advanced in time until a steady state is reached. Time steps $\Delta t = 0{\cdot}05, 0{\cdot}025$ and $0{\cdot}01$, were first tried for all the methods. It was found that PISO did not converge for $\Delta t = 0{\cdot}05$, while SMAC and SIMPLEC are stable for $\Delta t = 0{\cdot}05$.

The calculated steady-state radial and circumferential velocity components along the three radial lines $\theta = -20°$, $0°$ and $20°$ are compared with the experimental results of Fuchs and Tillmark[20] in Figures 3(a)–3(c). The numerical results obtained using all three methods with different time steps give near identical results in all cases and are in good agreement with the experimental results.[20]

Table I gives the computational effort required by the three methods to achieve steady state, where 'Time' is the non-dimensional time, 'Iterations' is the total number of time steps required and 'CPU' is the machine's CPU time in seconds. If the CPU time taken by the SMAC method is fixed as 1, then the CPU time is 1·7 for SIMPLEC and 1·89 for PISO for $\Delta t = 0{\cdot}05$. Figure 4 shows the time evolution of the average divergence $| e |^2$ and Figure 5 shows the maximum difference of the velocity components $| e |^3$ between two adjacent time levels. The evolution of the divergence reflects the accuracy of the numerical method and the evolution of the difference of the velocity components shows the convergence behaviour of the numerical method for a steady flow. From Figures 4 and 5 it is observed that the SIMPLEC method produces a smaller error in the continuity equation than the other methods at $\Delta t = 0{\cdot}05$. All three methods display almost equal convergence speed. However, since the SMAC method needs less computational time than SIMPLEC and PISO for each time step, it is the most efficient.

### *4.2. Laminar flow over a circular cylinder*

The flow over a circular cylinder has also been widely used as a test problem for numerical algorithms.[1,3,17] It is known experimentally that the flow is steady at $Re \leq 40$,[21,22] based on the

Table I. Computational effort for polar cavity flow at $Re = 350$

| Method | SMAC | | SIMPLEC | | PISO |
|---|---|---|---|---|---|
| $\Delta t$ | 0·05 | 0·01 | 0·05 | 0·01 | 0·025 |
| Time | 27·60 | 26·37 | 29·10 | 20·00 | 26·825 |
| Iterations | 552 | 2637 | 582 | 2000 | 1073 |
| CPU | 15114 | 24154 | 25949 | 28615 | 40386 |

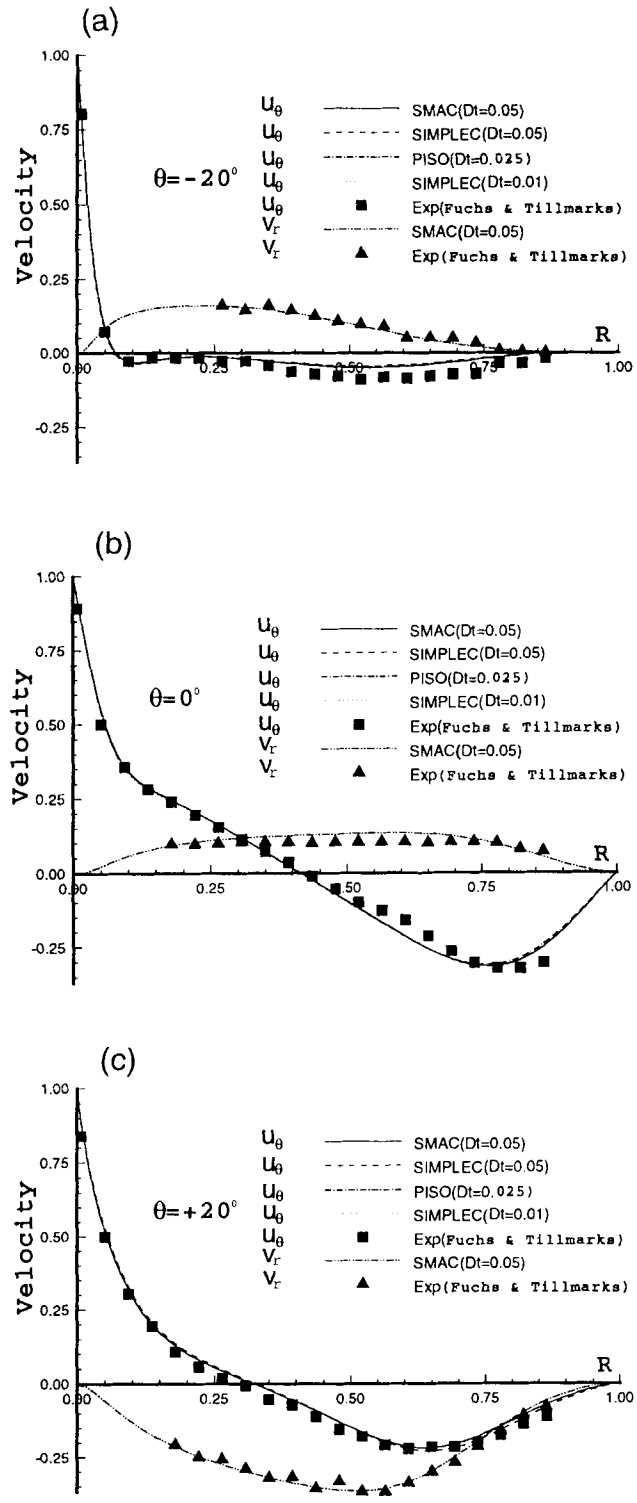


Figure 3. Velocity profiles of polar cavity flow with $Re = 350$ at (a) $\theta = -20°$, (b) 0° and (c) 20°

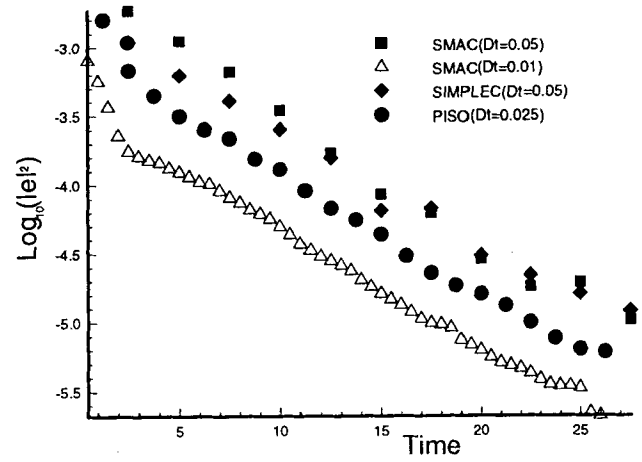


Figure 4. Evolution of the error norm $| e |^2$

diameter of the cylinder and the freestream velocity, and the flow is inherently unsteady when $Re > 40$. In order to validate the transient behaviour of the SMAC method, flows at $Re = 40, 100$ and 3000 have been simulated in the present study.

The flow around a circular cylinder is not confined in the physical domain; nevertheless, a finite external boundary is needed in order to obtain a numerical simulation. In the present study a $40r \times 60r$ rectangular region around the cylinder is taken as the computational domain, with the circular cylinder centre placed at $(20r,20r)$ and the left corner of the rectangular box as the origin, where $r$ is the radius of the cylinder. The domain is then discretized into a $100 \times 70$ grid with grid points clustered near the cylinder. The smallest grid size is $0{\cdot}15r \times 0{\cdot}15r$ and the largest $0{\cdot}87r \times 1{\cdot}1r$, giving a total of 7000 nodes. All the calculations are performed on this grid unless stated otherwise.

Experimental results on the time evolution of the separation length $L$ (measured from the rear of the cylinder and normalized by the diameter) at $Re = 40$ are available[21,22] and are compared with the

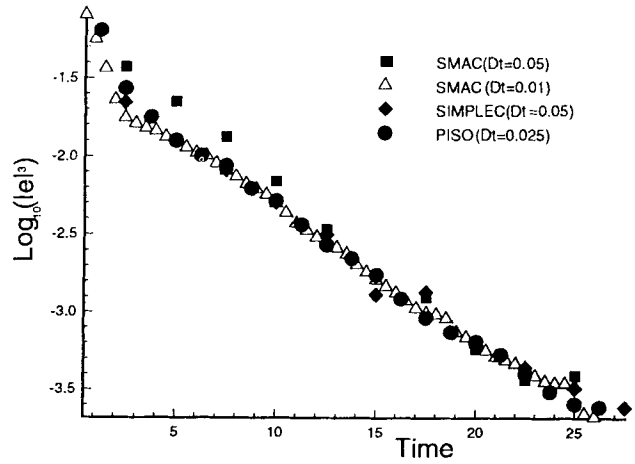


Figure 5. Evolution of the error norm $| e |^3$

Table II. Computational effort for flow around circular cylinder at $Re = 40$

| Method | SMAC | | SIMPLEC | | PISO | |
|---|---|---|---|---|---|---|
| $\Delta t$ | 0·05 | 0·025 | 0·05 | 0·025 | 0·05 | 0·025 |
| Time | 52·05 | 52·93 | 50·50 | 46·0 | 49·90 | 50·68 |
| Iterations | 1041 | 2117 | 1010 | 1840 | 998 | 2027 |
| CPU | 47986 | 72005 | 72725 | 116984 | 78450 | 125186 |
| CPU/iteration | 46·10 | 34·01 | 72·00 | 63·09 | 78·61 | 61·76 |

numerical results for the purpose of validating the transient behaviour of the SMAC, SIMPLEC and PISO schemes.

The calculations of the flow over a circular cylinder at $Re = 40$ were initially attempted with a time step $\Delta t = 0 \cdot 1$ for all three methods; however, none was convergent. The time step was then reduced to $\Delta t = 0 \cdot 05$ and 0·025, for which all three methods were convergent. The calculations were marched in time till a steady state was reached. Figure 6 presents a comparison of the numerical results and the experimental results of Coutanceau and Bouard[21] for the time evolution of the separation length behind the cylinder. The numerical results obtained using all three methods are equivalent and in good agreement with the experimental results. The steady state separation lengths predicted by the different methods are exactly the same. However, it is noted that a slight oscillation occurs in the later part of the transient solution for all the methods at $\Delta t = 0 \cdot 05$. These are reduced considerably in the solutions at $\Delta t = 0 \cdot 025$. Figure 7 shows the pressure distribution along the cylinder surface compared with the experimental results of Grove *et al.*[23] The pressure coefficient $C_p$ shown in the figure is defined as $Cp = (p - p_0 + \frac{1}{2}\rho U_0^2)/\frac{1}{2}\rho U_0^2$, where $p_0$ is the pressure at the front stagnation point of the cylinder and $\theta$ is zero at the front stagnation point. The pressure predicted by the SMAC method agrees very well with the experimental results as well as with the numerical results obtained by SIMPLEC and PISO. The fact that there are no pressure oscillations on the present non-staggered grid indicates that the elliptic correction technique used is effective. The flow pattern behind the cylinder is shown in Figure 8 using SMAC with $\Delta t = 0 \cdot 05$ when the computation has reached steady state. The symmetrical vortex pair behind the cylinder is clearly seen and the flow pattern is exactly the same as the experimental results given in Coutanceau and Bouard's work.[21]

Table II gives the computational effort required by the different methods to obtain steady state. It is seen again that the SMAC method is the most efficient. The ratio of the CPU time spent by SMAC, SIMPLEC and PISO for this problem is about $1:1 \cdot 5 : 1 \cdot 6$ respectively.

The flow over a circular cylinder at $Re = 100$ is unsteady and always accompanied by vortex shedding in the wake region. In order to generate the vortex shedding numerically at this Reynolds number, an artificial asymmetrical perturbation is introduced. The details of the artificial perturbation are discussed in Reference 17. The computational grid used is exactly the same as the one for $Re = 40$, with a time step $\Delta t = 0 \cdot 05$ used for all three methods. The time evolution of the lift coefficients predicted using SMAC, SIMPLEC and PISO is shown in Figure 9. The lift coefficient is defined as $C_L = \text{lift}/(0 \cdot 5\rho U_0^2 D)$, where $U_0$ is the freestream velocity and $D$ is the diameter of the cylinder. The periodic properties of the flow resulting from the vortex shedding are clearly seen in this figure. The calculated Strouhal numbers $St$ obtained from Figure 9 are compared with the numerical results of Kim

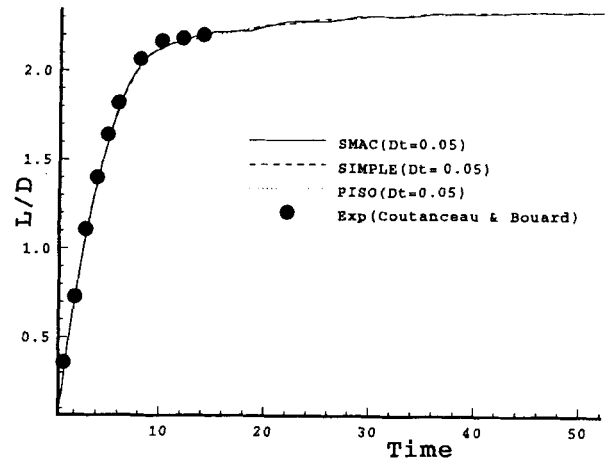


Figure 6. Time evolution of separation length behind circular cylinder at $Re = 40$

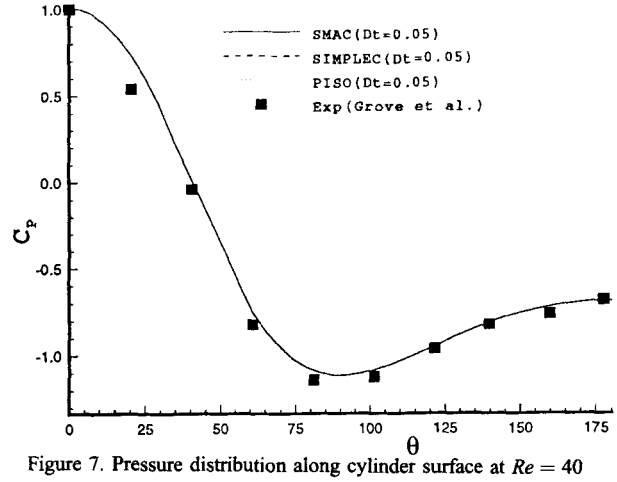


Figure 7. Pressure distribution along cylinder surface at $Re = 40$

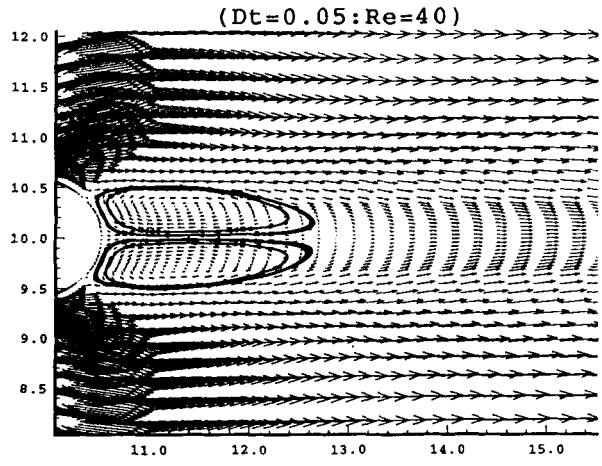


Figure 8. Velocity field behind circular cylinder at $Re = 40$

Table III. $St$-values ($St = 2fr/U_0$) for flow around circular cylinder, at $Re = 100$

| Method | | SMAC | SIM-PLEC | PISO | Experiment[17] |
|---|---|---|---|---|---|
| Kim and Benson[2] | $\Delta t$ | 0·05 | 0·05 | 0·05 | 0·160 |
| | $St$ | 0·155 | 0·158 | 0·164 | |
| Present | $\Delta t$ | 0·05 | 0·05 | 0·05 | |
| | $St$ | 0·158 | 0·159 | 0·158 | |

and Benson[1] and the experimental result summarized by Braza *et al.*[17] in Table III; good agreement is observed. The CPU times in seconds spent by SMAC, SIMPLEC and PISO when the calculation is advanced to dimensionless time $T = 100$ are 113,676, 159,030 and 201,123 respectively. The ratio of cpu time is 1:1·4:1·77 respectively and SMAC is again the most efficient of the methods. This conclusion is consistent with the results by Kim and Benson.[1]

The velocity vectors in roughly a single shedding period obtained using SMAC with $\Delta t = 0{\cdot}05$ are shown in Figures 10(a)–10(g). A small vortex with negative rotation attached to the upper cylinder grows and separates from the wall, while at the same time another vortex with the opposite rotation starts to grow on the lower side of the cylinder. As the negative rotation vortex is swept away by the freestream, the positive vortex continues to grow and itself separates and a new negative vortex begins to form on the upper part of the cylinder, completing one shedding cycle.

In order to validate the applicability of the SMAC method for flows with higher Reynolds numbers, the initial development of an impulsively started flow over a circular cylinder at $Re = 3000$ is simulated. The initial development of the flow at this Reynolds number has been studied experimentally by Bouard and Coutanceau[24] as an example to validate a numerical scheme for the study of oscillating flow around a circular cylinder.

This flow was calculated using an $80r \times 80r$ square computational domain with the circular cylinder centred at $(40r, 40r)$. The larger computational domain was chosen for this higher Reynolds number to ensure that boundary effects were negligible. The domain was discretized using a $175 \times 126$ non-rectangular mesh with grid points clustered near the cylinder surface and the downstream side. The

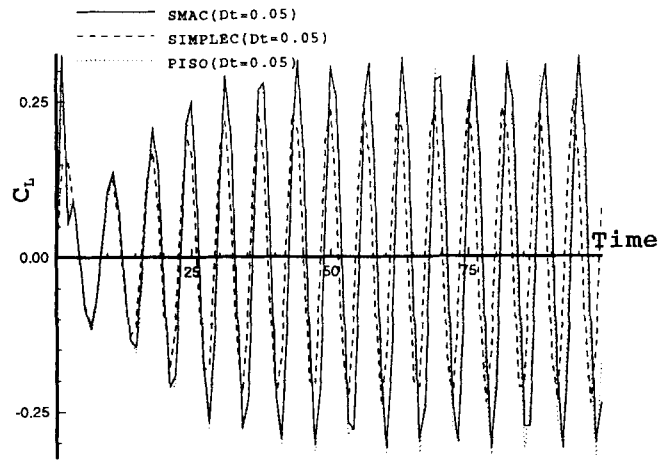


Figure 9. Evolution of lift coefficient for flow over a circular cylinder at $Re = 100$

cylinder surface is divided by 64 equally space grid points and the minimum grid size is approximately $0{\cdot}1r \times 0{\cdot}1r$, with $\Delta t = 0{\cdot}01$. Figure 11 shows a comparison of the calculated separated flow behind the cylinder at dimensionless time $t = 2{\cdot}5$ with the flow visualization result of Bouard and Coutanceau;[24] the agreement between the two results is excellent. Figure 12 shows the time evolution of the recirculation region length compared with the results from other studies; good agreement is again observed.

## 5. CONCLUSIONS

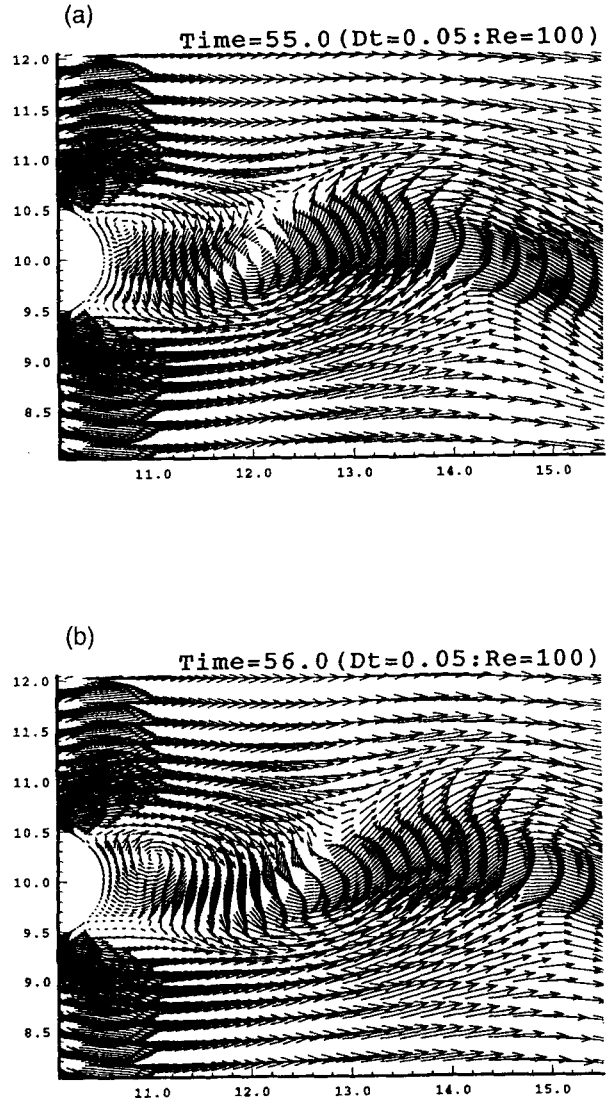


Figure 10. Velocity vectors for a vortex-shedding cycle at $Re = 100$ at various times shown in the figures

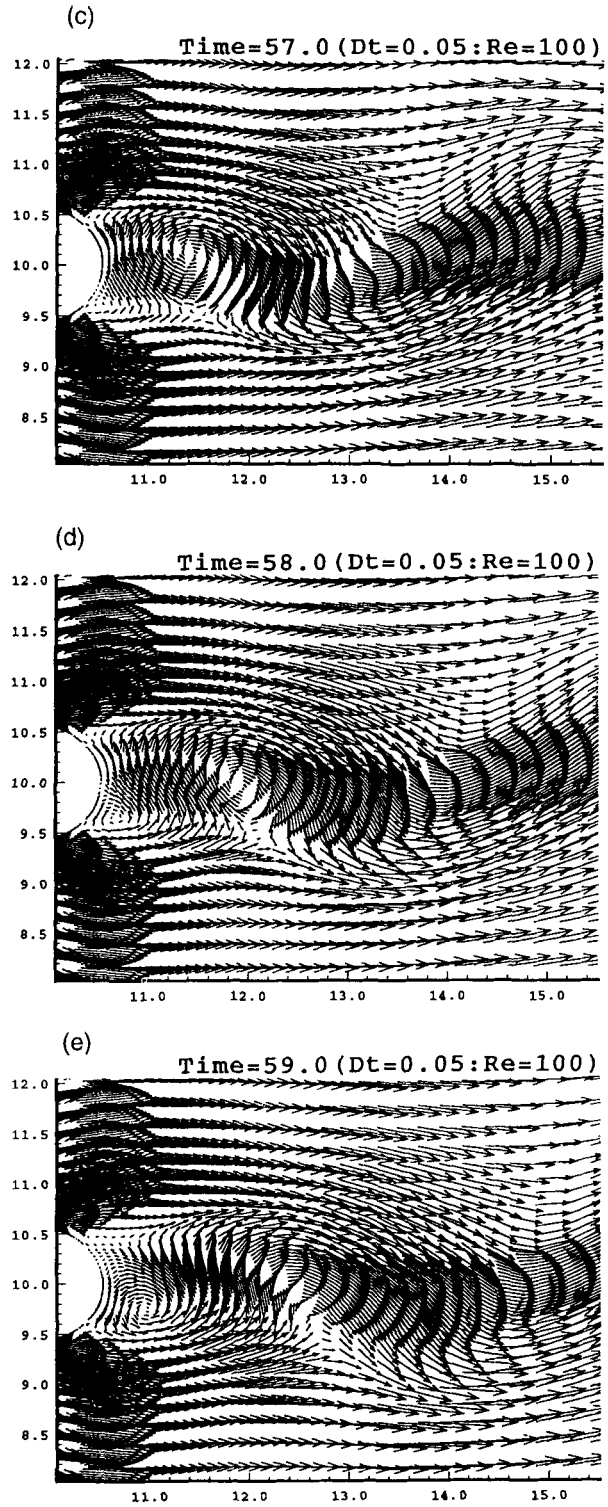


Figure 10. Velocity vectors for a vortex-shedding cycle at $Re = 100$ at various times shown in the figures

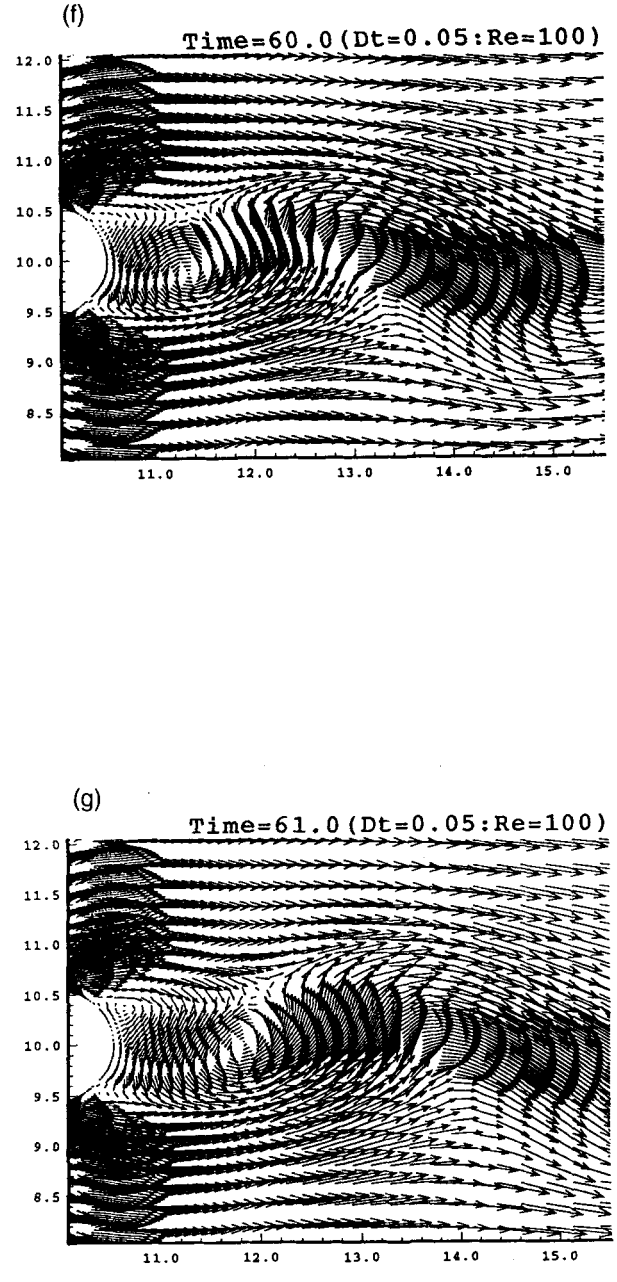


Figure 10. Velocity vectors for a vortex-shedding cycle at $Re = 100$ at various times shown in the figures

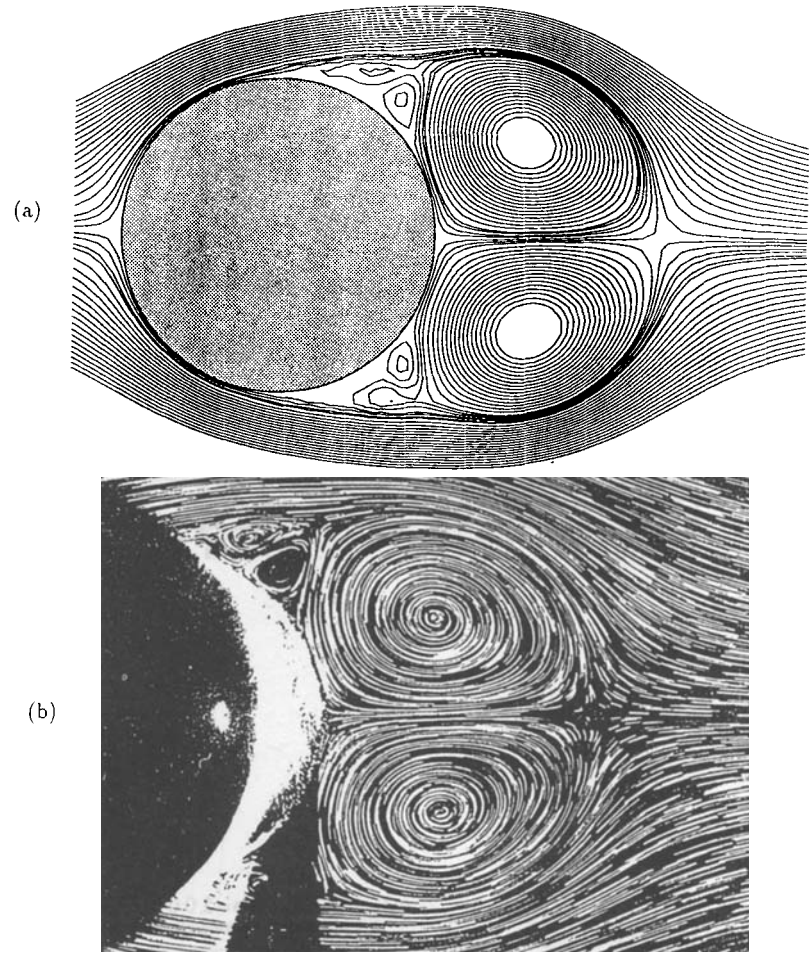


Figure 11. Recirculation zone for an impulsively started flow around a circular cylinder at $Re = 3000$ and $t = 5$: (a) present calculation visualized by streamfunction contours; (b) flow visualization result by Bouard and Coutanceau[24]

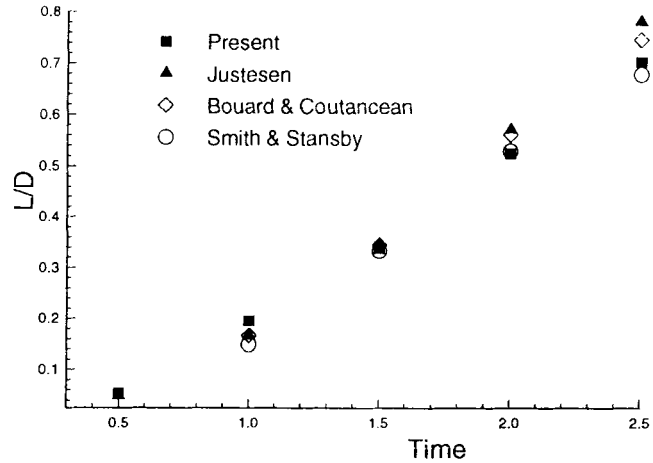


Figure 12. Time evolution of recirculation zone for an impulsively started flow around a circular cylinder at $Re = 3000$

A simplified marker and cell (SMAC) method for solving the unsteady incompressible Navier–Stokes equations on a non-staggered grid is presented in generalized curvilinear co-ordinates. Suppression of the pressure oscillations induced by the non-staggered grid arrangement is achieved by introducing an elliptic correction to the flux through the control volume faces in the continuity equation. Polar cavity flow and flows over a circular cylinder at Reynolds numbers of 40, 100 and 3000 are calculated and compared with both the numeral and experimental results. The following conclusions have been reached.

(1) The numerical results show that the elliptic correction works very well in suppressing the pressure oscillations on the non-staggered grid.
(2) The calculations of the polar cavity flow and the flow over a circular cylinder at $Re = 40$ show that the SMAC method is more efficient than the SIMPLEC and PISO methods for steady flows.
(3) The SMAC method is much more efficient than the SIMPLEC and PISO methods for unsteady flow, because although the same time step can be used for all three methods, the SMAC method needs less computational time than SIMPLEC and PISO for each time step.

## REFERENCES


1. S. -W. Kim and T. J. Benson, 'Comparison of the SMAC, PISO and iterative time-advancing schemes for unsteady flows', *Comput. Fluids*, **21**, 435–454 (1992).
2. M. Peric, R. Kessler and G. Scheuerer, 'Comparison of finite-volume numerical methods with staggered and colocated grids', *Comput. Fluids*, **16**, 389–403 (1988).
3. M. Rosenfeld, D. Kwak and Marcel, 'A fractional step solution method for the unsteady incompressible Navier–Stokes equations in generalized coordinate systems', *J. Comput. Phys.*, **94**, 102–137 (1991).
4. C. M. Rhie and W. L. Chow, 'Numerical study of the turbulent flow past an airfoil with trailing edge separation', *AIEE J.*, **21**, 1525–1532 (1983).
5. S. V. Patankar and D. B. Spalding, 'A calculation procedure for heat, mass and momentum transfer in three-dimensional parabolic flows', *Int. J. Heat Mass Transfer*, **15**, 1778–1806 (1972).
6. S. Majumdar, 'Role of underrelaxtion in momentum interpolation for calculation of flow with nonstaggered grids', *Numer. Heat Transfer*, **13**, 125–132 (1988).
7. W. Rodi, S. Majumdar and B. Schönung, 'Finite-volume methods for two-dimensional incompressible flows with complex boundaries', *Proc. 8th Int. Conf. on Computing Methods in Applied Sciences and Engineering*, Versailles, 1987.
8. M. Reggio and R. Camarero, 'Numerical solution procedure for viscous incompressible flows', *Numer. Heat Transfer*, **10**, 131–146 (1986).
9. F. H. Harlow and J. E. Welch, 'Numerical calculation of time-dependent viscous incompressible flow of fluid with free surface', *Phys. Fluids*, **8**, 2182–2189 (1965).
10. A. A. Amsden and F. H. Harlow, 'The SMAC method: a numerical technique for calculating incompressible fluid flows', *Los Alamos Scientific Report LA-4370*, 1970.
11. R. I. Issa, 'Solution of the implicitly discretized fluid flow equations by operator-splitting', *J. Comput. Phys.*, **62**, 40–65 (1985).
12. J. P. Van Doormal, 'Enhancements of the SIMPLE method for predicting incompressible fluid flows', *Numer. Heat Transfer*, **7**, 147–163 (1984).
13. S. W. Armfield, 'Finite difference solution of the Navier–Stokes equations on staggered and non-staggered grids', *Comput. Fluids*, **20**, 1–17 (1991).
14. S. W. Armfield, 'Ellipticity, accuracy and convergence of the discrete Navier–Stokes equations', *J. Comput. Phys.*, **114**, 176–184 (1994).
15. J. F. Thompson, F. C. Thames, R. L. Walker and S. P. Shank, 'Numerical solution of the unsteady Navier–Stokes equations for arbitrary bodies using boundary-fitted curvilinear coordinates', *Proc. Arizona/AFOSR Symp. on Unsteady Aerodynamics*, University of Arizona, 1975.
16. B. P. Leonard, 'A stable accurate convective modelling procedure based on quadratic upstream interpolation', *Comput. Methods in Appl. Mech. Eng.*, **19**, 59–98 (1979).
17. M. Braza, P. Chassaing and H. Haminh, 'Numerical study and physical anlaysis of the pressure and velocity fields in the near wake of a circular cylinder', *J. Fluid Mech.*, **165**, 79–130 (1986).
18. S. V. Patankar, *Numerical Heat Transfer and Fluid Flow*, Hemisphere, Washington, DC, 1980.
19. P. M. Gresho, 'Some current CFD issues relevant to the incompressible Navier–Stokes equations', *Comput. Methods Appl. Mech. Eng.*, **87**, 201–252 (1991).
20. L. Fuchs and N. Tillmark, 'Numerical and experimental study of driven flow in a polar cavity', *Int. j. numer. methods fluids*, **5**, 311–329 (1985).

21. M. Coutanceau and R. Bouard, 'Experimental determination of the main features of the viscous flow in the wake of a circular cylinder in uniform translation. Part 1. Steady flow', *J. Fluid Mech.*, **79**, Pt. 2, 231–256 (1977).
22. M. Coutanceau and R. Bouarde, 'Experimental determination of the main features of the viscous flow in the wake of a circular cylinder in uniform translation. Part 2. Unsteady flow', *J. Fluid Mech.*, **79**, Pt. 2, 257–272 (1977).
23. A. S. Grove, F. H. Shair, E. E. Petersen and A. Acrivos, 'An experimental investigation of the steady separated flow past a circular cylinder', *J. Fluid Mech.*, **19**, 60–80 (1964).
24. R. Bouard and M. Coutanceau, 'The early stage of development of the wake behind an impulsively started cylinder for $10 < Re < 10^4$', *J. Fluid Mech.*, **101**, Pt. 3, 583–607 (1980).
25. P. A. Smith and P. K. Stansby, 'Impulsively started flow around a circular cylinder by the vortex method', *J. Fluid Mech.*, **194**, 45–77 (1988).
26. P. Justesen, 'A numerical study of oscillating flow around a circular cylinder', *J. Fluid Mech.*, **222**, 157–196 (1991).